



EDEN: Flare Activity of the Nearby Exoplanet-hosting M Dwarf Wolf 359 Based on K2 and EDEN Light Curves

Chia-Lung Lin¹, Wen-Ping Chen¹, Wing-Huen Ip^{1,2,3}, Dániel Apai^{4,5}, Alex Bixel⁴, Richard Boyle⁶, Jose Perez Chavez⁷, Nestor Espinoza⁸, Aidan Gibbs⁹, Paul Gabor⁶, Thomas Henning¹⁰, Luigi Mancini^{10,11,12}, Benjamin V. Rackham^{13,14}, Martin Schlecker¹⁰, Jeremy Dietrich⁴, Quentin Jay Socia⁴, Miriam Keppler¹⁰, Asmita Bhandare¹⁰, and Maximilian Häberle¹⁰

¹ Graduate Institute of Astronomy, National Central University, Taoyuan 32001, Taiwan

² Graduate Institute of Space Science, National Central University, Taoyuan 32001, Taiwan

³ Space Science Institute, Macau University of Science and Technology, Macau

⁴ Steward Observatory, 933 N Cherry Avenue, Tucson, AZ 85721, USA

⁵ Lunar and Planetary Laboratory, 1629 E. University Boulevard, Tucson, AZ 85721, USA

⁶ Vatican Observatory Research Group, University of Arizona, 933 N Cherry Avenue, Tucson, AZ 85721-0065, USA

⁷ Steward Observatory, 933 N. Cherry Avenue, Tucson, AZ 85721, USA

⁸ Space Telescope Science Institute, 3700 San Martin Drive, Baltimore, MD 21218, USA

⁹ Department of Physics & Astronomy, University of California, Los Angeles, Los Angeles, CA 90095, USA

¹⁰ Max-Planck-Institut für Astronomie, Königstuhl 17, Heidelberg D-69117, Germany

¹¹ Department of Physics, University of Rome Tor Vergata, Via della Ricerca Scientifica 1, I-00133 Rome, Italy

¹² INAF—Turin Astrophysical Observatory, Via Osservatorio 20, I-10025 Pino Torinese, Italy

¹³ Department of Earth, Atmospheric and Planetary Sciences, and Kavli Institute for Astrophysics and Space Research, Massachusetts Institute of Technology, Cambridge, MA 02139, USA

Received 2020 August 30; revised 2021 April 5; accepted 2021 April 15; published 2021 June 11

Abstract

We report the flare activity of Wolf 359, the fifth closest star to the Sun and a candidate exoplanet-hosting M dwarf. The star was a target of the Kepler/K2 mission and was observed by the EDEN project, a global network of 1–2 m class telescopes for detection and characterization of rocky exoplanets in the habitable zones of late-M dwarfs within 50 light year from the solar system. In the combination of the archived K2 data and our EDEN observations, a total of 872 flares have been detected, 861 with the K2 (860 in the short-cadence and 18 in the long-cadence data, with 17 long-cadence events having short-cadence counterparts) and 11 with EDEN. Wolf 359 has relatively strong flare activity even among flaring M dwarfs, in terms of the flare activity indicator (FA) defined as the integrated flare energy relative to the total stellar bolometric energy, where $FA = \sum E_f / \int L_{bol} dt \sim 8.93 \times 10^{-5}$ for the long-cadence flares, whereas for K2 short cadence and EDEN flares, the FA values are somewhat larger, $FA \approx 6.67 \times 10^{-4}$ and $FA \approx 5.25 \times 10^{-4}$, respectively. Such a level of activity, in accordance with the rotation period (P_{rot}), suggests the star to be in the saturation phase. The size of the starspots is estimated to be at least $1.87\% \pm 0.59\%$ of the projected disk area of Wolf 359. We find no correlation of FA with the stellar rotational phase. Our analysis indicates a flare frequency distribution in a power-law form of $dN/dE \propto E^{-\alpha}$ with $\alpha = 2.13 \pm 0.14$, equivalent to an occurrence rate of flares $E_f \geq 10^{31}$ erg about once per day and of superflares with $E_f \geq 10^{33}$ erg approximately 10 times per year. These superflares may impact the habitability of system in multiple ways, the details of which are topics for future investigations.

Unified Astronomy Thesaurus concepts: Planet hosting stars (1242); Exoplanet systems (484); Exoplanet astronomy (486); Exoplanets (498); Flare stars (540); Stellar flares (1603); Stellar phenomena (1619)

Supporting material: machine-readable tables

1. Introduction

Due to the dynamo mechanism, magnetic field can be continuously generated in stars. The magnetic energy built up is released in an explosive manner in the form of stellar flares via the reconnection process. This effect is well studied in the case of the Sun (Shibata & Magara 2011). From ground-based observations, it is known that, among the low-mass stars, the M dwarfs like YZ CM (dM4.5e), EV Lac (dM3.5e), and AD Leo have far more frequent flare occurrence rates than G-type stars (Hawley & Pettersen 1992; Kowalski et al. 2010). The photometric measurements with the Kepler space telescope with unprecedented high precision have provided a wealth of information on the M dwarfs following the important discovery of the superflares with energy exceeding that of the largest solar

flares on record (Maehara et al. 2012; Hawley et al. 2014; Wu et al. 2014; Chang et al. 2017, 2018; Davenport et al. 2019; Lin et al. 2019). The interest in such phenomena is partly motivated by the habitability of exoplanets hosted by M dwarfs. That is, the habitable zones of M dwarfs are generally very close to the host stars such that their atmospheres could be subject to extreme space weather and erosion effects because of strong interactions with the stellar coronal mass ejections and energetic irradiation (e.g., Aarnio et al. 2012; Airapetian et al. 2017).

Although innovative and revolutionary, the observations in the Kepler prime mission were limited by the fact that most of the target stars are relatively distant, therefore only powerful flares with energy exceeding 10^{31} erg could be detected. To study the flare-generation mechanism and compare with solar flares, it is desirable to examine flares on lower energy scales. This difficulty could be overcome by studying nearby stars. As one of the

¹⁴ 51 Pegasi b Fellow.

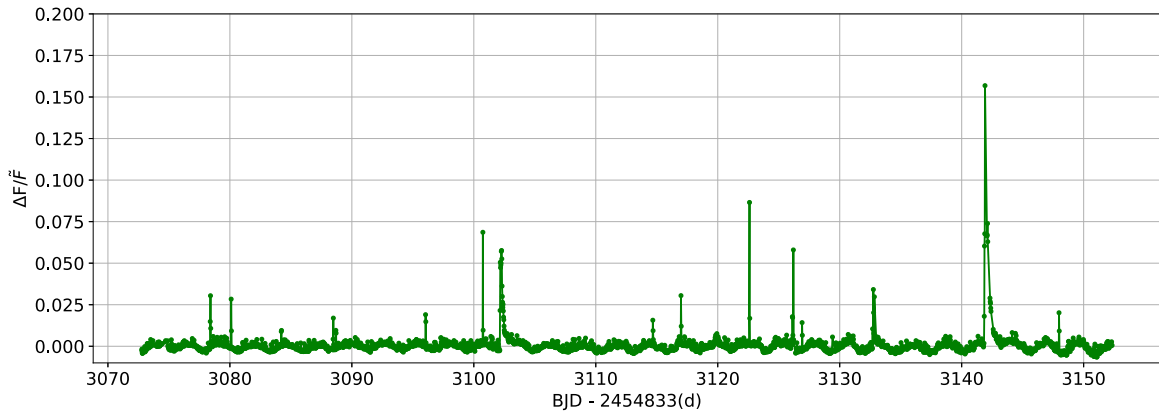


Figure 1. The K2 LC light curve of Wolf 359 obtained in Campaign 14.

Table 1
The Properties of Wolf 359

Designations	Spec. Type	Radius (R_{\odot})	T_{eff} (K)	P_{rot} (day)	Distance (pc)	Age (Myr)
GJ 406 EPIC 201885041 ^a CN Leonis	M5.5 ^b M6 ^c	0.16 ^d	2800 ± 100 ^e	2.72 ± 0.04 ^f	2.42 ^g	<500 ^h

Notes.

^a The name used in the K2 Survey.

^b From Reid et al. (1995).

^c From Kirkpatrick et al. (1991).

^d From Doyle & Butler (1990).

^e From Fuhrmeister et al. (2005) and Pavlenko et al. (2006).

^f From Guinan & Engle (2018).

^g From Weinberger et al. (2016).

^h From Engle & Guinan (2018).

nearest late-type active M dwarfs, Wolf 359 (CN Leonis, GJ 406, see Table 1), at a distance of 2.42 pc (Weinberger et al. 2016) and of spectral type M5.5 (Reid et al. 1995) to M6 (Kirkpatrick et al. 1991), is ideal for this purpose. In addition to its relevance for astrophysics, Wolf 359—as the fifth closest star to the Sun—is also a notable system in popular culture, and it is featured in many science fiction stories and movies, such as Star Trek. Indeed, recent radial velocity measurements revealed that Wolf 359 is a planet host (Tuomi et al. 2019), although its habitable zone has not yet been thoroughly explored.

With a surface temperature of 2700–2800 K (Fuhrmeister et al. 2005) to 2900 K (Pavlenko et al. 2006) and various band magnitudes, such as $B = 15.541$, $V = 13.507$, $R = 11.684$, and so on, Wolf 359 has a rotation period of 2.72 ± 0.04 days (Guinan & Engle 2018), indicative of a young gyrochronological age <500 Myr (Engle & Guinan 2018). Like other late-type M dwarfs, the star has a strong surface magnetic field, on the order of 2.4 kG (Reiners & Basri 2007). Its flare activity has been monitored over a wide wavelength range from radio, optical, to X-ray emissions. For example, Fuhrmeister et al. (2007, 2008, 2010) and Lefke et al. (2010) reported simultaneous ground-based spectroscopic (UVES/Very Large Telescope: 3000–10000 Å) and space-borne (XMM/Newton: 0.2–10 keV) observations of a number of major flares of Wolf 359 in 2004 and 2005, for which the X-ray fluxes increased by a factor of 100 from the quiescent level. Large responses could also be detected in the chromospheric line emissions.

Hawley et al. (2014) investigated in detail the short-cadence (SC; 1 minute) light curves of active versus inactive M dwarfs with Kepler observations and compared the strengths and occurrence rates of their flare activities according to the

respective flare frequency distributions. Wolf 359 was classified as one of the hyperflaring stars (see Chang et al. 2018; Lin et al. 2019). Guinan & Engle (2018) analyzed the corresponding K2 data obtained in Campaign 14. Its minimum flare energy was limited to be about 10^{31} erg as only long-cadence (LC; 30 minutes) data were used. A full picture of the origin and generation mechanism of the magnetic energy release and dissipation is thus hampered by this detection limit. In this study we supplement the analysis of Guinan & Engle (2018) by using K2 SC and ground-based observations with larger aperture telescopes and shorter cadence; we are thereby able to detect flares with energy down to about 10^{29} erg. In the subsequent sections, the ground-based observations were presented together with a demonstration of how a wider energy coverage can provide a deeper understanding of the magnetic activity of this nearby star.

2. Observations

Wolf 359 was observed by the Kepler space telescope in Campaign 14 of the K2 mission from 2017 June 1 to 2017 August 19. Kepler/K2 data contain two types of primary flux information, simple aperture photometry (SAP) flux with 1σ uncertainties and the SAP with removal of artificial/systematic noise called presearch data conditioning SAP (PDCSAP) flux with 1σ uncertainties (see Smith et al. 2012; Stumpe et al. 2012). The PDCSAP light-curve data obtained in LC (30 minutes) were first reported in Guinan & Engle (2018), which explored its flare activity over this 3-month interval (Figure 1). Note that the K2 LC light curve shown in Figure 1 is a bit different from that displayed in Guinan & Engle (2018)

Target ID: 201885041, Cadence: 4348901

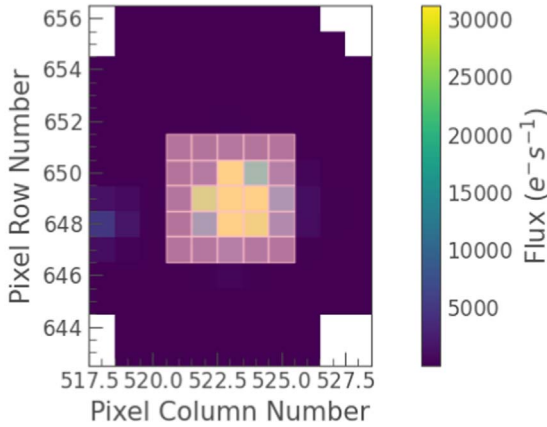


Figure 2. An arbitrary cadence of K2 SC target pixel data of Wolf 359. The area covered by transparent white is the aperture used to extract the light curve.

because the data points with bad quality (flag bits `SAP_QUALITY` $\neq 0$) have been excluded.

Besides the LC data, Wolf 359 was also observed in SC of 1 minute with the data available only in target pixel files (TPFs). In order to extract the SC light curve, the Python package `Lightkurve` for Kepler/K2 and TESS data analyses (Lightkurve Collaboration et al. 2018) were employed to perform photometry. Figure 2 shows an example of the TPF data and the optimal aperture used to produce the light curve. Note that the raw light curve is contaminated by systematic noise caused by thruster firings and spacecraft motion that were removed by using the self flat fielding method (Vanderburg & Johnson 2014), which is also included in the `Lightkurve` package. The final SC light curve is shown in Figure 3

Wolf 359 is also one of the red dwarf targets of interest to the EDEN project (Gibbs et al. 2020) in the search for habitable planets. While the main scientific goal of EDEN, by using a coordinated network of 1–2 m class telescopes, is to identify and characterize transiting habitable exoplanets orbiting late-M stars within 50 lt-yr, the high-cadence EDEN light curves are also useful to study stellar variability studies. The partnership of EDEN includes the Department of Physics of the University of Rome “Tor Vergata”; the Steward Observatory of the University of Arizona; the Max-Planck-Institut für Astronomie, Germany; the Vatican Observatory; and the Lulin Observatory of National Central University, Taiwan (EDEN PIs are: D. Apai, P. Gabor, Th. Henning, and W-P. Chen). There were three separate observing sessions of Wolf 359, one contributed by the VATT 1.83 m telescope in the V band on 2019 January 30 and the other two by the Kuiper 1.54 m telescope in the R band on 2019 February 25 and 27. The total observation time was 16 hr with cadences of 30–45 s. Figure 4 exhibits the EDEN light curves from these three observation sessions. Because of the shorter cadences of the EDEN and K2 SC observations compared with that of the K2 LC observations (1 minute vs. 30 minutes), flares at lower levels not detectable by K2 LC would be accessible for the present analysis. Our work combines these three complementary sets of data to diagnose the flare activity of Wolf 359.

3. Data Analysis

3.1. Flare Detection

The K2 light curves of Wolf 359 exhibit small-amplitude variations arising from surface spots modulated by stellar rotation. These low-amplitude, slow modulations are occasionally interrupted by rapid brightening due to stellar flares. To quantify the flares, Lin et al. (2019) developed an algorithm to generate a flare-free light curve, from which individual flares could be identified, by subtraction from the original light curve. In this way, 18 and 860 flares are recognized in the K2 LC and SC data of Campaign 14, respectively, and 17 of the LC flares have SC counterpart detection. One LC flare has no counterpart in the SC data because of a short data gap (no. 13 in Figure 5) in the SC light curve. Since the LC data flag shows the good quality of the data points of this flare, it was kept as a detected event with a note. As a result, 861 flare events have been detected in total (see Figure 5).

A flare amplitude profile describing the brightness increase in excess of the nominal stellar luminosity is a function of time and can be expressed as

$$\frac{\Delta F(t)}{\bar{F}} = \frac{F(t) - \bar{F}}{\bar{F}}, \quad (1)$$

where $F(t)$ is the flux as a function of time in the optical emission of a flare and \bar{F} is the median of quiescent flux of a star. Figure 6 shows a summary of the flare profiles in the K2 LC light curve as well as their counterparts in the SC data of Wolf 359. For the EDEN light-curve data given in magnitude as the unit of brightness, $\Delta F(t)/\bar{F}$ is calculated by using the following equation

$$\frac{\Delta F(t)}{\bar{F}} = 10^{\frac{\Delta m(t)}{-2.5}} - 1, \quad (2)$$

where $\Delta m(t)$ is the corresponding difference between the magnitude of a flare and the median value of the stellar magnitude at quiescent state.

Figure 7 elaborates on the EDEN flares by using an analysis algorithm that is just slightly different from that used on the K2 data. The procedure used to generate the flare-free curve on the EDEN’s data is briefly explained here: First, an N -point moving median curve is produced, with $N=5$ being the optimal value. Second, the N -point curve is generated from the original curve in order to produce a residual curve. Third, the median absolute deviation of the residual curve is calculated. Fourth, every data point in the original curve with its counterpart in the residual curve being larger than X times of median absolute deviation will be discarded. The optimal value of the variable X for every light curve is found by visually examining the flare-free curve obtained with different values. For example, for VATT’s observation on 2019 February 27, $X=0.08$, and for Kuiper’s observations on 2019 January 30 and February 25, $X=0.5$. The data gaps due to this step are filled in by interpolation. At this point, an artificial light curve is obtained, but it may not be completely flare free. Finally, the same procedure as above is repeated on the artificial curve using the same $N=5$ and corresponding X value. The resulting flare-free curves are shown in Figures 7(a), (c), and (e). We found that there is no need to iterate three times because it will not make any distinct difference. Eleven flare events in these EDEN observations are detected this way.

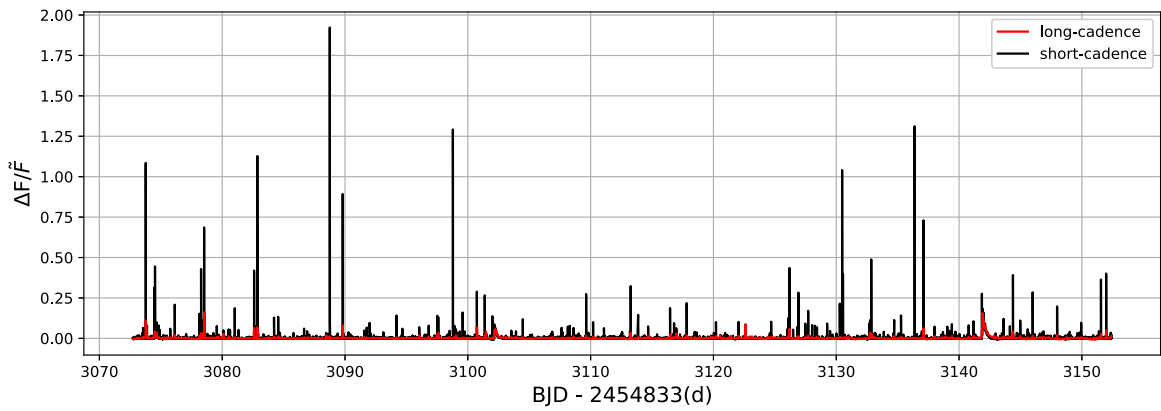


Figure 3. The SC light curve (black) of Wolf 359. The LC light curve (red) is drawn for comparison.

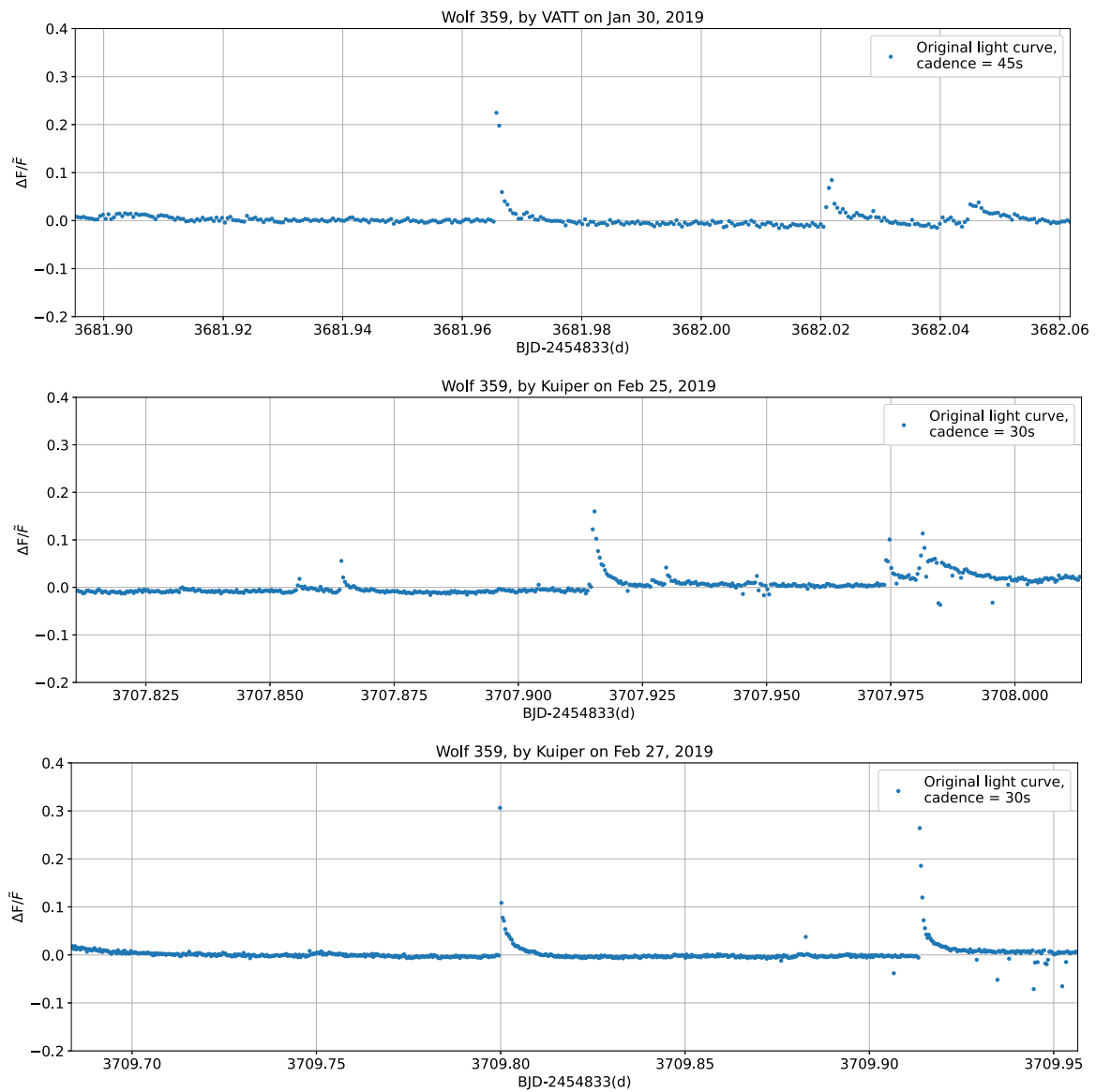


Figure 4. The light curves of Wolf 359 produced by the project EDEN. The upper one was observed by the VATT 1.82 m telescope on 2019 January 30. The middle and bottom ones were observed by the Kuiper 1.54 m telescope on 2019 February 25 and 27, respectively.

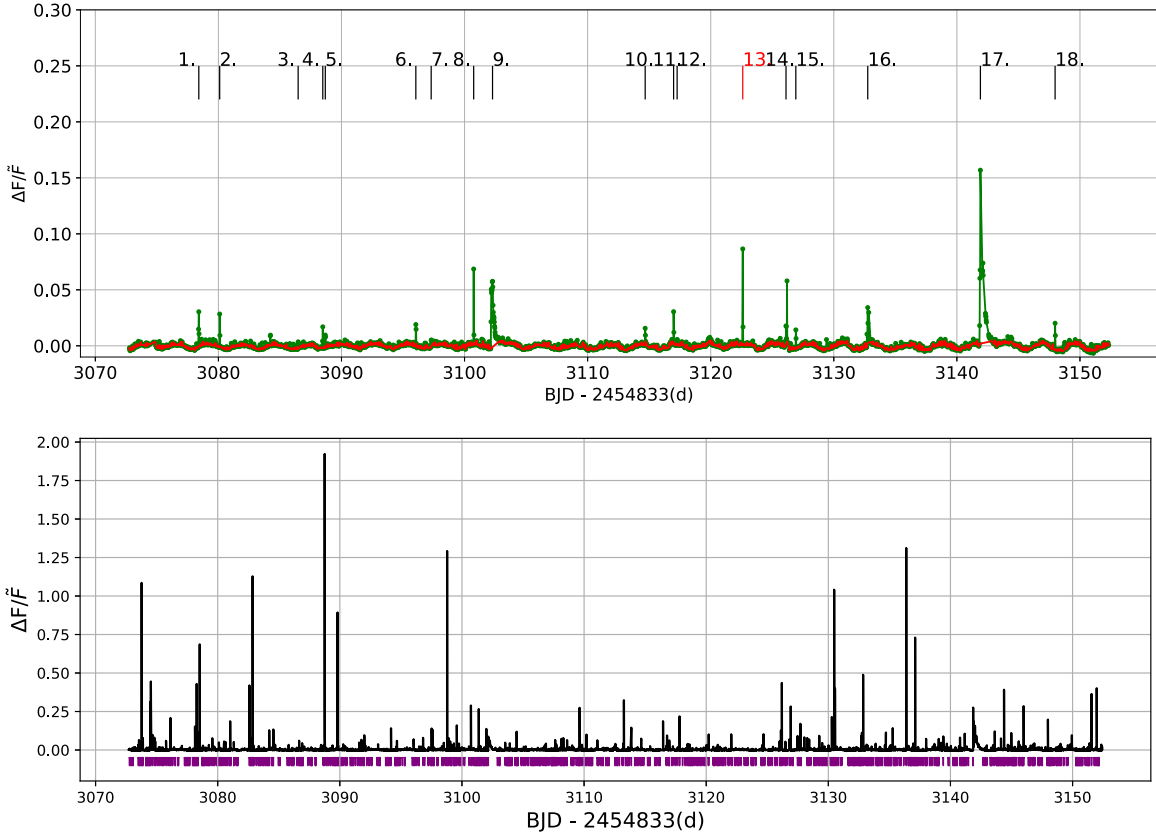


Figure 5. Upper panel: the K2 LC light curve of Wolf 359 and the flare-free curve (red). The vertical lines with numbers mark the timing of 18 flares detected using our algorithm in the light curve. The 13th flare marked in red has no counterpart in the SC observation. Lower panel: 860 flares detected in the K2 SC light curve are marked with the purple vertical lines. In total, 861 flares are found in the K2 observations.

3.2. Flare Energies

An equivalent duration (ED) is defined as follows (Gershberg 1972):

$$\text{ED} = \int \frac{\Delta F(t)}{\bar{F}} dt. \quad (3)$$

It is the amount of time required for the nonflaring star to emit the same amount of energy as the cumulative energy of the given flare. Therefore, ED can be used to calculate the energy of the flare by multiplying it by the quiescent stellar flux in the telescope bandpass (Vida et al. 2017)

$$E_{f,\lambda} = \text{ED} \times F_{*,\lambda}, \quad (4)$$

and the corresponding quiescent stellar flux of Wolf 359 can be estimated from

$$F_{*,\lambda} = 4\pi R_*^2 \sigma T_*^4 f_\lambda(T_*). \quad (5)$$

Here the stellar radius $R_* = 0.16 R_\odot$, the effective temperature $T_* = 2800$ K for Wolf 359, σ is the Stefan–Boltzmann constant, and f_λ is a bandpass response factor as a function of temperature for the wavelength (λ) band. The response factor functions of the bands used in the study, that is, V, R for EDEN, and Kepler bands, are shown in Figure 8.

In order to better synthesize these events observed in different bands, the bandpass energy can be converted to the bolometric energy using the following equation, based on the

approximation given by Howard et al. (2018):

$$E_f = \frac{E_{f,\lambda}}{f_\lambda(T_f)}. \quad (6)$$

Here the E_f is the bolometric flare energy and T_f is the flare temperature. The two-band simultaneous flare observations carried out by Howard et al. (2020) suggested that the flare temperature increases with the energy of the flare. Nevertheless, such a relationship is not evident for the M dwarfs with mass $< 0.52 M_\odot$ (see Figure 9), with which the bolometric energies were converted from the energies in g' band used by Evryscope using Equation (6) with the corresponding estimated flare temperature. Instead, the M dwarf flare temperatures follow a Gaussian distribution in logarithmic scale, and an average value of $T_f = 7780_{-1740}^{+2241}$ K can be obtained using the least-square fitting. In the following, this mean temperature value is used to convert the bandpass flare energies of the above samples into the bolometric energies.

4. Results and Discussions

Table 2 lists EDEN flare parameters, such as the flare peak amplitude (A_f), flare energy in band ($E_{f,\lambda}$), bolometric flare energy (E_f), the time of the brightest peak (t_{max}), and duration (τ_f) of these flare events, sorted by E_f from the weakest to the strongest. The parameters of K2 LC flares and their SC counterparts are listed in Table 3. The parameters of the first 20 K2 SC flares are also given in Table 4, and the full table is available in machine-readable format.

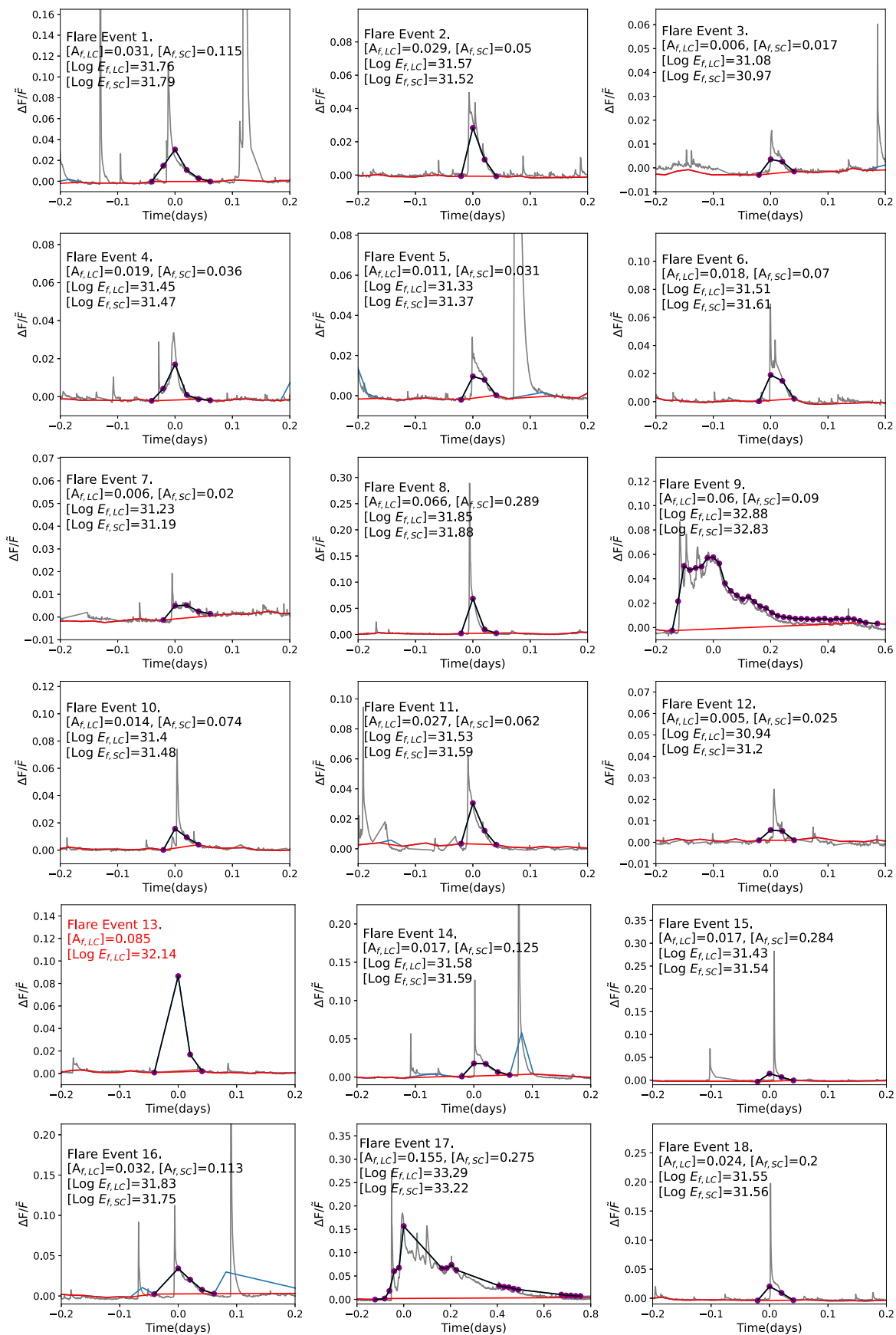


Figure 6. The profiles of the 18 K2 LC flares. The 13th one, which has no SC counterpart, is noted with the red caption in the panel. The red curve represents the flare-free curve. The blue curve is the K2 LC light curve, and the SC light curve is shown in gray. Many of the K2 LC flares are the complex events resolved by the SC observations.

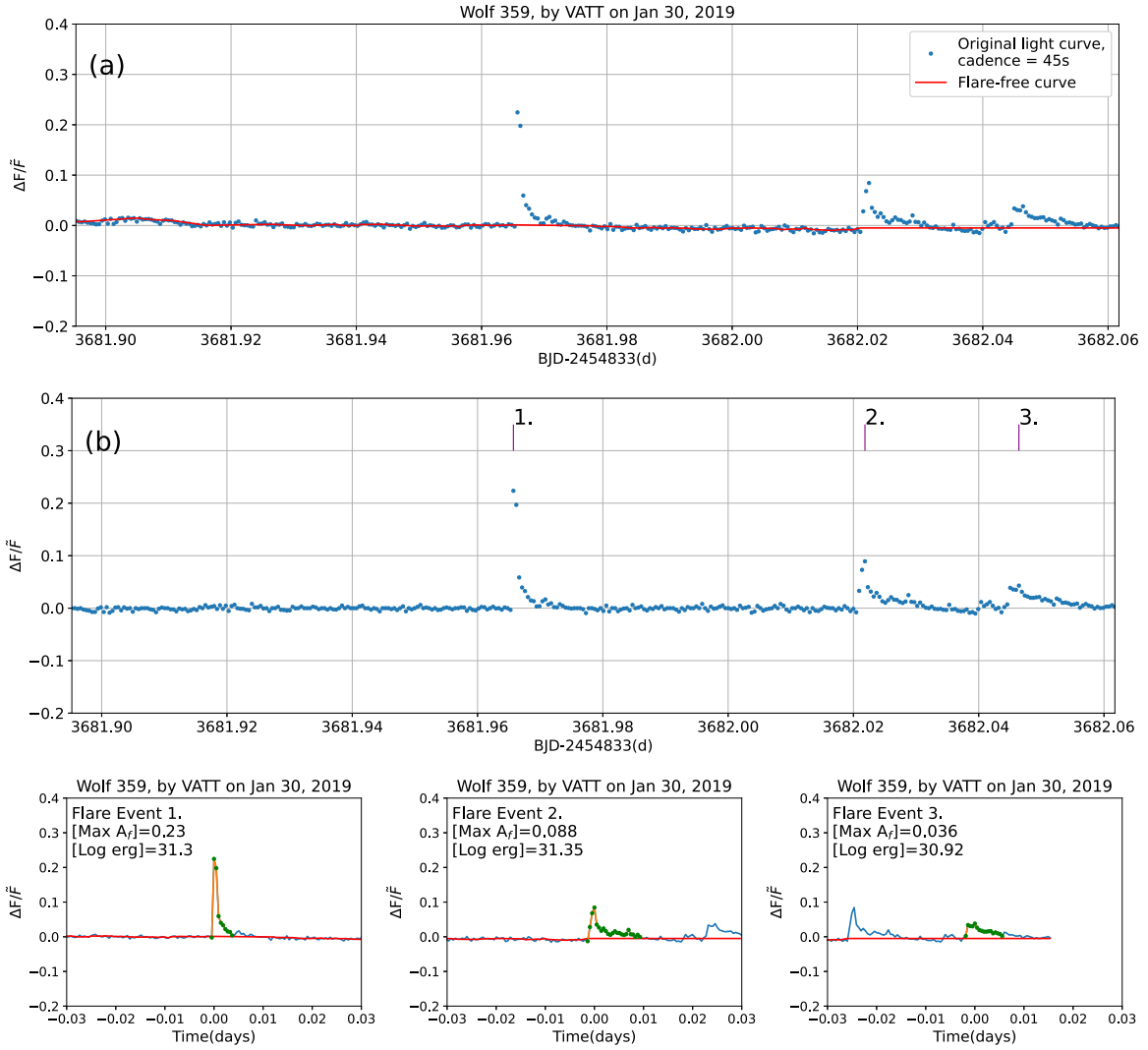


Figure 7. (1) Flares detected by VATT on 2019 January 30. (2) Flares detected by Kuiper on 2019 February 25. (3) Flares detected by Kuiper on 2019 February 27. The steps of searching for flares using a similar algorithm presented in Lin et al. (2019; see Section 3) in the light curves observed by VATT on January 30 (1), Kuiper on February 25 (2), and February 27 (3), 2019. The upper subpanel shows the original light curve (blue) and the flare-free curve (red). The middle subpanel is the residual curve produced by subtracting the flare-free curve from the original curve. The rest of subpanels show the profiles of detected flares in each observation.

The largest A_f is 0.311 for the flare detected on 2019 February 27 in the EDEN data, whereas the minimum A_f is 0.015 on 2019 February 25. In the K2 data, the largest peak amplitude of the LC flares is 0.155, while the smallest value is 0.005. Their SC counterparts show a complex structure composed of multiple small flares with $A_f=0.276$ and 0.025, respectively. The brightest SC flare with $A_f=1.92$ and $E_f=1 \times 10^{33}$ erg has no LC counterpart because a data point during the event was probably excluded by the Kepler pipeline in the archival LC light curve. The A_f of the faintest SC flare is 0.003.

The most energetic event of Wolf 359 detected by K2 is no. 17 in Figure 6, with $E_f \approx 1.64 \times 10^{33}$ erg in SC and $E_f \approx 1.93 \times 10^{33}$ erg in LC. The E_f of the weakest K2 LC flare is about 8.7×10^{30} erg; the flare was also detected in SC data with $E_f \approx 1.57 \times 10^{31}$ erg. An SC flare with $E_f \approx 1.78 \times 10^{29}$ erg is the weakest event detected in this study.

In total, 17 flares were detected in both the SC and LC data. The LC flare peak amplitudes are obviously underestimated, being only $32\% \pm 17\%$ of those estimated by the SC data. However, the flare energies derived from both the LC and SC

data are almost the same. The LC flare energy to SC energy ratio is on average 0.97. This may be due to the underestimated amplitude and overestimated duration of the LC flares (Raetz et al. 2020). In short, combining these observations, Wolf 359 is found to be able to generate flares with E_f in a range of $\sim 2 \times 10^{29}$ to 2×10^{33} erg.

Due to the faster sampling capability, the EDEN observations are supposed to see small flares beyond the K2 SC detection limit. Nevertheless, probably due to the photometric accuracy, the weakest flare detected by EDEN on Wolf 359 was $E_f \approx 2.6 \times 10^{30}$ erg—stronger than the weakest flare K2 SC observed. It is noted that the measurements A_f and E_f are subject to the finite cadence of the observations, and hence they are just the lower limits of the true peak amplitudes and energies.

4.1. Flare Activity

To examine the flare activity level of Wolf 359 more quantitatively, we use the normalized flare energy, FA (Yang et al. 2017), as the indicator. FA is defined by the summation of energies of all detected flares ($\sum E_f$) divided by the total stellar

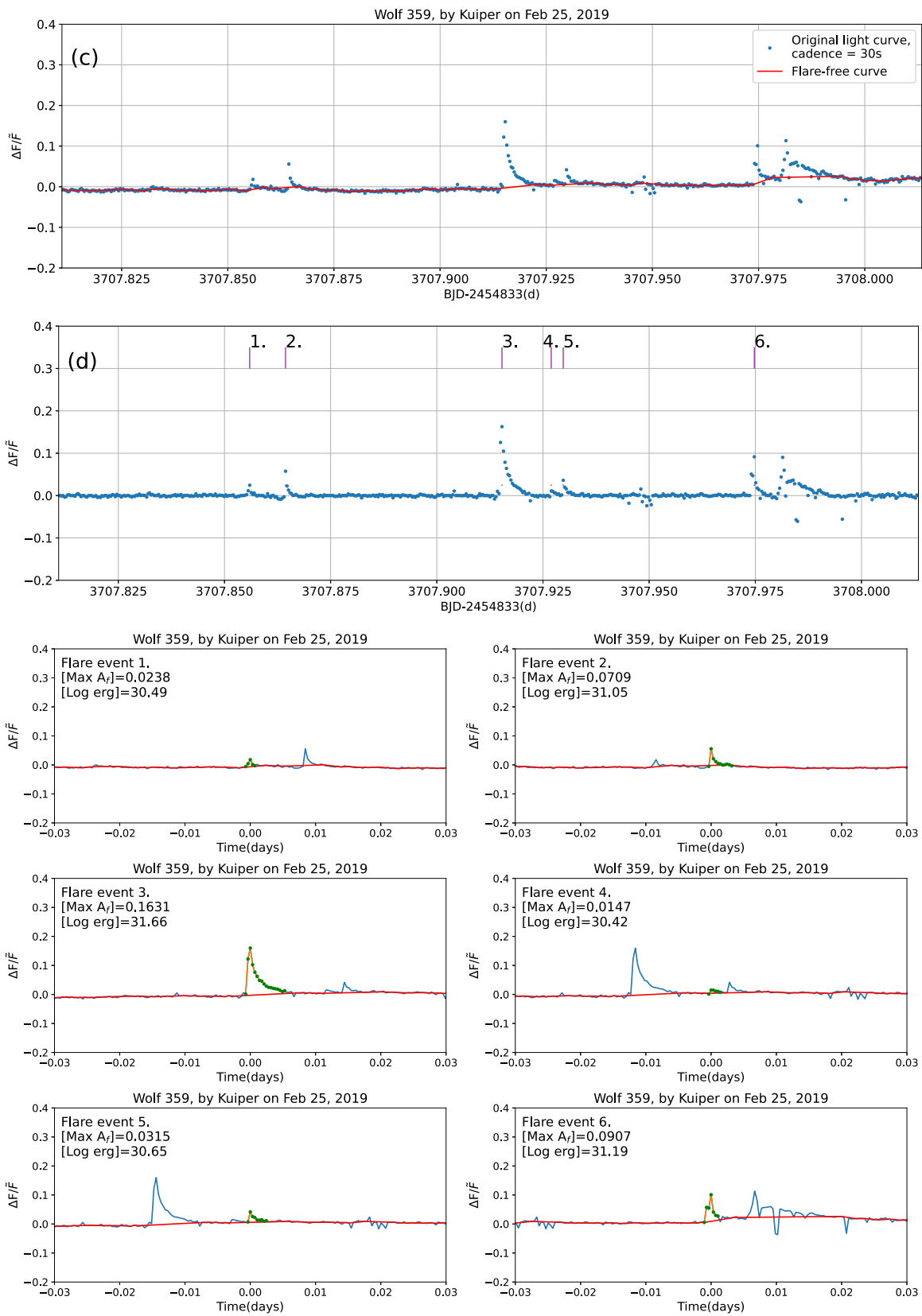


Figure 7. (Continued.)

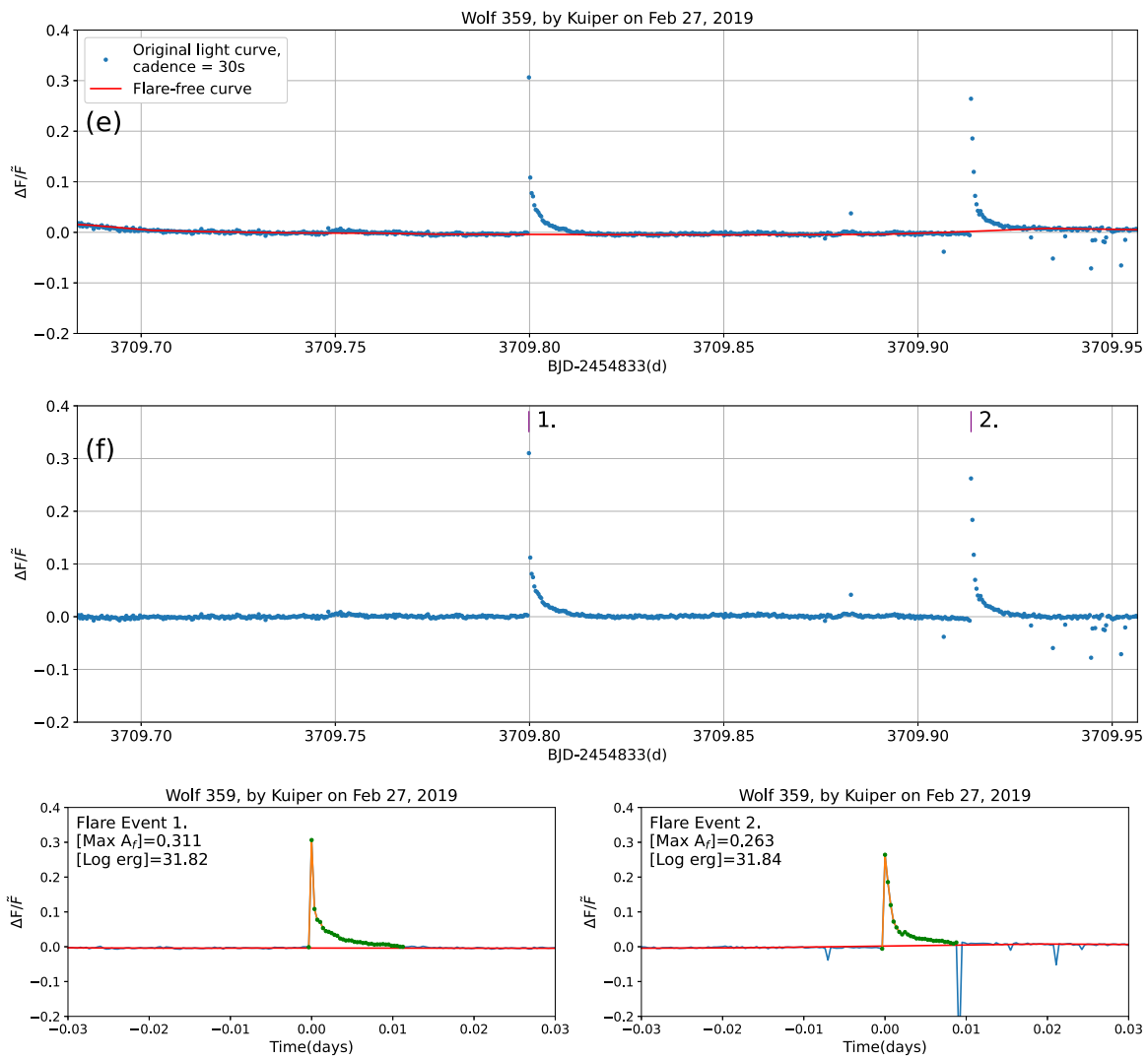


Figure 7. (Continued.)

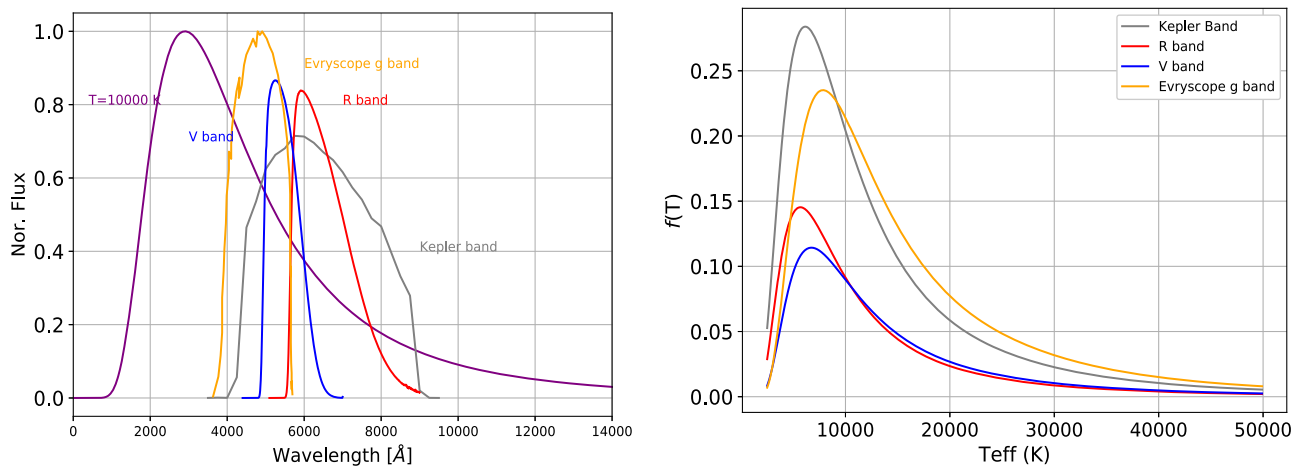


Figure 8. The left panel shows the response functions of V (blue), R (red), and Kepler (gray) bands used by the observations in this study and the 10,000 K blackbody radiation in purple for a comparison. The Evryscope g' band (Howard et al. 2020) is also shown in yellow. The right panel displays the response factor functions, f_{λ} , of these bands.

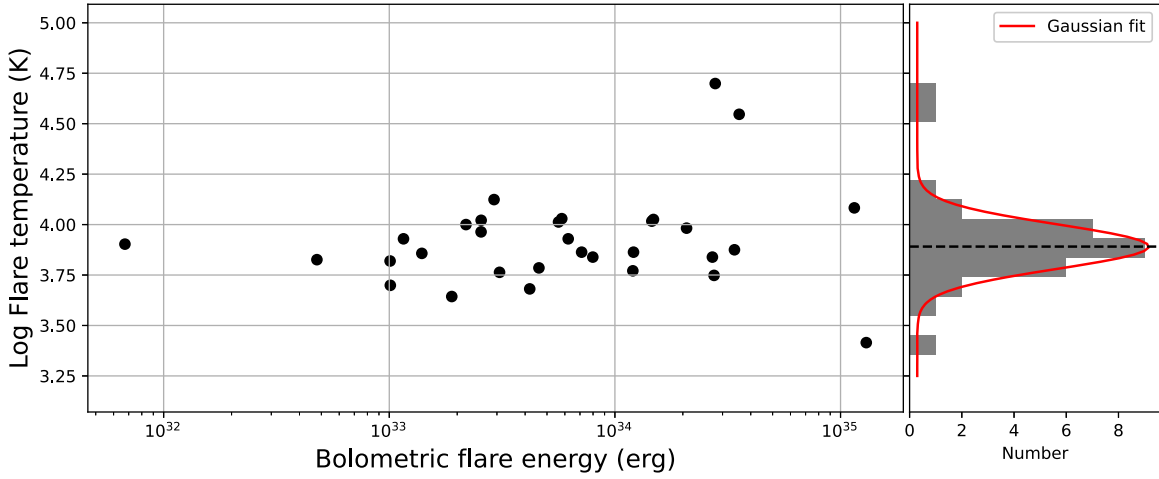


Figure 9. The flare temperatures vs. the bolometric energies of the stars with the mass lower than $0.52 M_{\odot}$ (M dwarfs). These data originated from the observation carried out by Howard et al. (2020). The bolometric energies are converted from g' band energies given by Howard et al. (2020) using Equation (6). It can be seen that the flare temperature does not depend significantly on flare energy for M dwarfs. Instead, it follows a normal distribution regardless of flare energy, as shown on the right subpanel. The black dashed horizontal line represents the mean value derived from the best-fit Gaussian function, and on average a flare temperature with 1σ standard deviation, $T_f = 7780_{-1740}^{+2241}$ K, can be obtained.

Table 2
The Flares Observed on Wolf 359 by EDEN in This Study

A_f	$E_{f,\lambda}$ Log(erg)	E_f Log(erg)	t_{\max} (BJD-2,454,833)	τ_f (hr)
0.0147	29.51	30.42	3707.926951	0.0337
0.0238	29.59	30.49	3707.855936	0.0337
0.0315	29.75	30.65	3707.929764	0.0422
0.0358	29.97*	30.92	3682.046418	0.1894
0.0709	30.14	31.05	3707.864371	0.0506
0.0908	30.29	31.19	3707.974762	0.0506
0.2304	30.34*	31.30	3681.965721	0.1113
0.0877	30.39*	31.35	3682.021841	0.2669
0.1631	30.75	31.66	3707.915347	0.1097
0.3111	30.92	31.82	3709.799833	0.2867
0.2628	30.93	31.84	3709.913663	0.2277

Note. The columns are (1) flare peak amplitude (A_f) and (2) flare energy in the used band λ ($E_{f,\lambda}$). The ones marked with * were observed in the V band, and the rest were in R band. (3) Bolometric flare energy (E_f), (4) time of flare peak (t_{\max}), and (5) duration of flare (τ_f).

(This table is available in machine-readable form.)

bolometric luminosity emitted for the whole observation period ($\int L_{\text{bol}} dt$):

$$\text{FA} = \frac{\sum E_f}{\int L_{\text{bol}} dt} \quad (7)$$

for Wolf 359. The FA value of our EDEN observations is about 6.66×10^{-4} , while a value of 5.25×10^{-4} is derived from K2 SC flares. On the other hand, K2 LC flares obtain a smaller value of 8.93×10^{-5} , suggesting that the effect of the small flares, which cannot be resolved in the LC observation, is significant for such measurements. In comparison, the FA values obtained by Kepler LC observations for flaring M dwarfs vary between 2.24×10^{-5} and 4.69×10^{-5} (Yang et al. 2017; Lin et al. 2019), indicating that Wolf 359 is magnetically quite active. According to Yang et al. (2017), in the FA – P_{rot} relationship, where P_{rot} is the rotation period, flaring M dwarfs can be classified into three phases of activity: supersaturation

($P_{\text{rot}} \lesssim 1$ day), saturation ($1 \text{ day} \lesssim P_{\text{rot}} \lesssim 4$ day), and exponential decay ($P_{\text{rot}} \gtrsim 4$ day). M dwarfs' flare activities first increase with the increase of spin rate in the exponential decay phase. Then, in the saturation phase, flare activities stop increasing with the acceleration of spin rate. When rotation periods are shorter than about 1 day, in the supersaturation phase the flare activities become slightly weaker than in the saturation phase. Given that both the rotational period (2.7 days) and its activity level (as measured in units of FA) are in the intermediate ranges, Wolf 359 is clearly a star in the saturation region.

4.2. Relation between Flares and Starspots

It has been suggested that most of stellar flares occur near starspots, where the magnetic flux is much stronger, with a fraction of the stored magnetic energy released as the flare energy (Maehara et al. 2012). The starspot fractional coverage area, $A_{\text{spot}}/A_{\text{star}}$, can be determined by using the following equation (Maehara et al. 2017):

$$\frac{A_{\text{spot}}}{A_{\text{star}}} = \left(\frac{\Delta F}{F} \right)_{\text{spot}} \left[1 - \left(\frac{T_{\text{spot}}}{T_*} \right)^4 \right]^{-1}, \quad (8)$$

where A_{star} is the area of the stellar disk and T_* and T_{spot} are the temperature of the star and the starspot, respectively. Berdyugina (2005) reported that T_* and T_{spot} are correlated and that this correlation can be fit well by the following relationship:

$$\begin{aligned} \Delta T(T_*) &= T_* - T_{\text{spot}} \\ &= 3.58 \times 10^{-5} T_*^2 + 0.249 T_* - 808. \end{aligned} \quad (9)$$

It can therefore be determined that the T_{spot} of Wolf 359's spot region is about 2630 K. Note that the data Berdyugina (2005) fit probably had significant scatter and lack the cool stellar samples with the temperatures as cool as Wolf 359, so this derived value for W359 is probably not as precise as the stated value here suggests. The $(\Delta F/F)_{\text{spot}}$ in Equation (8) is the brightness variation amplitude of the rotation modulation caused by the starspots. Its value is calculated by following

Table 3
The K2 LC Flares and Their SC Counterparts

$A_{f,LC}$	$E_{f,Kp,LC}$ Log(erg)	$E_{f,LC}$ Log(erg)	$t_{max,LC}$ (BJD-2,454,833)	$\tau_{f,LC}$ (hr)	$A_{f,SC}$	$E_{f,Kp,SC}$ Log(erg)	$E_{f,SC}$ Log(erg)	$t_{max,SC}$ (BJD-2,454,833)	$\tau_{f,SC}$ (hr)
0.0307	31.18	31.76	3078.408920	2.452	0.1149	31.21	31.79	3078.397001	2.043
0.0291	30.98	31.57	3080.104806	1.471	0.0496	30.94	31.52	3080.098335	1.030
0.0060	30.50	31.08	3086.479671	1.471	0.0165	30.39	30.97	3086.481374	0.850
0.0191	30.87	31.45	3088.482023	2.452	0.0359	30.89	31.47	3088.479639	2.239
0.0109	30.75	31.33	3088.686345	1.471	0.0309	30.78	31.37	3088.685323	1.210
0.0181	30.93	31.51	3096.041888	1.471	0.0700	31.02	31.61	3096.041548	1.765
0.0056	30.65	31.23	3097.288239	1.961	0.0203	30.61	31.19	3097.283131	1.602
0.0664	31.26	31.85	3100.741238	1.471	0.2885	31.30	31.88	3100.735449	1.700
0.0601	32.29	32.88	3102.273630	17.653	0.0896	32.25	32.83	3102.156828	15.986
0.0142	30.82	31.40	3114.675739	1.471	0.0738	30.89	31.48	3114.679485	2.305
0.0273	30.94	31.53	3116.984525	1.471	0.0618	31.01	31.59	3116.976012	1.504
0.0048	30.35	30.94	3117.270569	1.471	0.0250	30.61	31.20	3117.276358	2.517
0.0852	31.56	32.14	3122.603243	1.961
0.0165	31.00	31.58	3126.117491	1.961	0.1251	31.01	31.59	3126.119193	1.373
0.0166	30.85	31.43	3126.914326	1.471	0.2844	30.96	31.54	3126.922158	2.681
0.0316	31.25	31.83	3132.757781	2.452	0.1134	31.17	31.75	3132.751992	1.569
0.1551	32.70	33.29	3141.911167	21.085	0.2754	32.63	33.22	3141.859066	18.830
0.0239	30.97	31.55	3147.979380	1.471	0.1997	30.98	31.56	3147.981082	1.079

Note. The columns are (1) flare peak amplitude (A_f), (2) flare energy in the Kepler band, Kp ($E_{f,Kp}$), (3) bolometric flare energy (E_f), (4) time of flare peak (t_{max}), and (5) duration of flare (τ_f). The columns with the notation *LC* are for K2 LC flares, and with the notation *SC*, their K2 SC counterparts.

(This table is available in machine-readable form.)

Table 4
The Flares Detected by K2 SC Observations of Wolf 359

A_f	$E_{f,Kp}$ Log(erg)	E_f Log(erg)	t_{max} (BJD-2,454,833)	τ_f (hr)	In LC?
0.0073	30.49	31.08	3072.782163	1.030	No
0.0029	29.05	29.63	3072.873428	0.098	No
0.0033	29.63	30.21	3072.947666	0.212	No
0.0148	30.31	30.89	3073.009645	0.327	No
0.0031	29.37	29.95	3073.072986	0.114	No
0.0353	30.54	31.12	3073.506836	0.392	No
0.0659	30.82	31.40	3073.557236	0.588	No
0.0089	29.80	30.38	3073.598782	0.278	No
0.0070	29.61	30.19	3073.655312	0.163	No
0.0315	31.01	31.60	3073.721377	1.112	No
1.0853	31.95	32.53	3073.772459	1.079	No
0.0057	30.10	30.69	3073.834437	0.294	No
0.0059	29.92	30.50	3073.851464	0.360	No
0.0786	31.24	31.82	3073.872578	0.817	No
0.0034	29.91	30.49	3074.108914	0.327	No
0.0037	29.90	30.48	3074.153865	0.343	No
0.0168	30.31	30.89	3074.189963	0.392	No
0.0061	29.57	30.15	3074.228784	0.196	No
0.0057	29.50	30.08	3074.286676	0.163	No
0.0034	29.82	30.40	3074.323455	0.327	No

Note. The columns are (1) flare peak amplitude (A_f), (2) flare energy in the Kepler band, Kp ($E_{f,Kp}$), (3) bolometric flare energy (E_f), (4) time of flare peak (t_{max}), and (5) duration of flare (τ_f), and this is the flare also observed in the LC observations (in LC?). Only the first 20 K2 SC flares are presented in the table. The full table of Wolf 359's 861 K2 SC flares is available in machine-readable format.

(This table is available in its entirety in machine-readable form.)

the step-by-step procedure: (1) folding the light curves of Wolf 359 with its rotation period, that is, the phase curve; (2) binning the phase curve with an interval of 0.1 phase and estimating the mean values for all bins; (3) conducting a sine

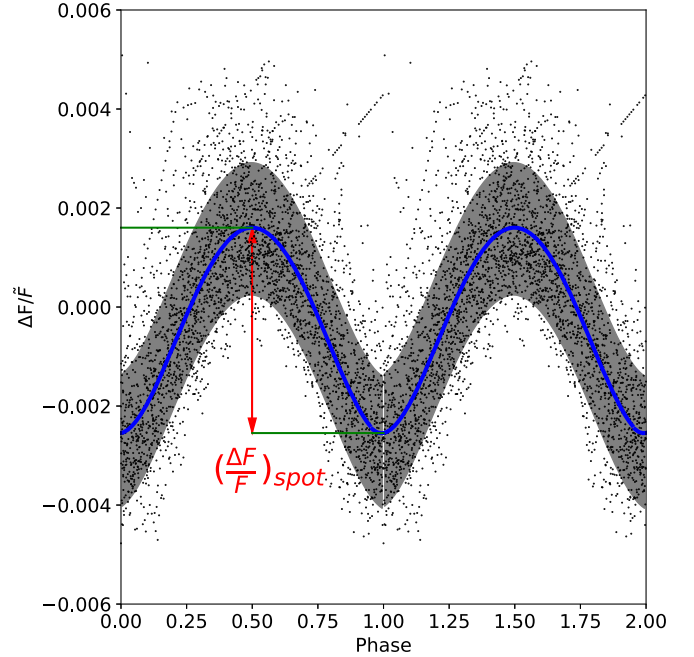


Figure 10. The phase curve of Wolf 359. The blue solid curve is a best-fit sinusoidal function of the phase curve. The $(\Delta F/F)_{spot}$ is the difference between the brightest and dimmest phase in the light curve. The gray filled region represents the 1σ brightness variation envelope.

wave fit of the mean values; (4) calculating the difference between the maximum and minimum values returned by the sinusoidal function at the given phases. We obtain a $(\Delta F/F)_{spot}$ value of 0.0041 ± 0.0013 for Wolf 359 (Figure 10).

As a result, the total area of starspots A_{spot} can be estimated to be $1.87\% \pm 0.59\%$ of Wolf 359's apparent disk. Because the inclination of the stellar rotational axis is not taken into account and some spots could be uniformly distributed, the estimated

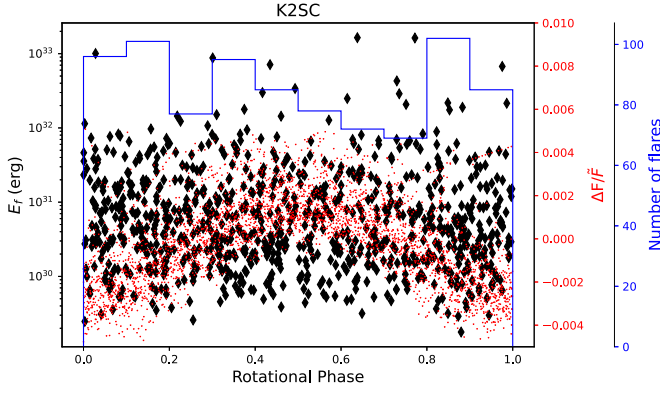


Figure 11. The relationship between rotational phase and flare. The folded K2 LC light curve is displayed in red. The flare energies are presented in black rhombuses, and the number distribution is presented in the blue histogram. No correlations between flare generation/energy and rotational phase for Wolf 359 are found from our data.

area may therefore be underestimated. This is well explained in Rackham et al. (2018). Moreover, there are not only starspots located at the active regions on the stellar surface but also bright spots, that is, faculae, which can also contribute to the uncertainty of the spots area estimation. In short, this fractional spot size we derived for Wolf 359 here is just a lower limit.

From statistics of the rotational phases of K2 SC flares in each 0.1 phase bin (see Figure 11), no apparent correlations between rotational phase and the flares’ number and energies can be found. Using K2 SC and TESS data, Doyle et al. (2018, 2019) also found the lack of preference for rotational phase in other flaring M dwarfs. They proposed three scenarios to explain this interesting finding. The first scenario suggests that the magnetic field interaction between the star and a stellar binary companion increases magnetic activity and produces flares outside the primary star’s active spot region. However, a small separation between the star and the companion would be required for this type of magnetic interaction. In the 80-day K2 observation of Wolf 359, there is no signature of periodic brightness dimming caused by any stellar companion candidate. Moreover, the radial velocity measurements of Wolf 359 carried out by Tuomi et al. (2019) with HARPS and HIRES did not detect any second companion (here referring to stellar companion) either, and hence the case of Wolf 359 is unlikely to be explained by this scenario.

The second scenario is star–planet interaction. Wolf 359 has two candidate exoplanets, Wolf 359 b ($M_p \sin i \sim 44M_{\oplus}$ and $a \sim 1.8$ au) and Wolf 359 c ($M_p \sin i \sim 3.8M_{\oplus}$ and $a \sim 0.018$ au), as inferred by RV measurements (Tuomi et al. 2019). The absence of transit signals from these planets in the light curves is probably because their orbital inclinations are so oblique that they would never cross in front of the host’s disk. The other possibility is that the ultraflare activity contaminates the transit signals, making them undetectable. The candidate planet Wolf 359 c is very close to Wolf 359, and its orbital period of $2.68687^{+0.00039}_{-0.00031}$ days is similar to the rotation period of its host (~ 2.72 days), suggesting possible spin–orbit coupling between them.

Third, fully convective low-mass stars such as Wolf 359 have been shown to be able to hold high-latitude starspots by theoretical model (i.e., Yadav et al. 2015). The flares detected in this study for Wolf 359 might be produced by the high-latitude or polar starspots, which could not be distinguished

from the light curve depending on the viewing geometry and inclination of the stellar rotational axis.

Furthermore, it is possible that the rotational modulations cannot reveal the active spots region due to the presence of faculae. The luminous faculae could compensate or surpass the dimming caused by starspots. There is also a potential for the presence of uniformly distributed small spots, which could contribute to flare generation as efficient as the dominant spots region (whether a large spot or a large region covered by concentrated small spots) that causes the rotational modulations.

4.3. Flare Frequency Distribution

A star’s flare activity behavior can be described in terms of its flare frequency distribution. Wolf 359’s flare frequency distribution is presented in Figure 12, as well as that of rapidly rotating ($P_{\text{rot}} < 10$ days) and hence young M dwarfs from the K2 LC flare study carried out by Lin et al. (2019) for comparison.

The different behaviors between K2 LC and K2 SC are mainly because of the difference in the sampling rates such that flares of smaller energy ($E_f < 10^{33}$ erg) will be increasingly missed by the LC measurements. At the same time, the profiles of flares with energy $< 10^{31}$ erg will not be detectable because of the very low values of the peak flare amplitudes. In comparison, the SC measurements provide information on flares with a detection limit as low as 2×10^{29} erg. Because of the limited observation time, the EDEN observations do not cover flare energy $> 10^{32}$ erg. The detection cutoff at flare energy $\sim 2 \times 10^{30}$ erg is likely caused by photometric precision.

A star’s flare frequency distribution can be indicated by a linear relation expressed in logarithmic form as

$$\log N = a + \beta \log E, \quad (10)$$

where N is the cumulative frequency of flares with a released energy E . The coefficient β represents the slope of the flare frequency distribution and suggests the property of the flare activity of the star. If a star is found to have $\beta < -1$, most of total energy emitted by the flares will be contributed by the small flares. For a star with $\beta > -1$, the stronger flares dominate the energy output.

$$dN \propto E^{-\alpha} dE, \quad (11)$$

where dN is the number of flares with the energies in the range of E and $E + dE$ and $\alpha = 1 - \beta$ (Hawley et al. 2014). We use the maximum likelihood estimator derived by Clauset et al. (2009) for α :

$$\alpha = 1 + n \left[\sum_{i=1}^n \ln \frac{E_i}{E_{\min}} \right]^{-1}, \quad (12)$$

and the error for α can be estimated by

$$\sigma_{\alpha} = \frac{\sqrt{n+1}(\alpha-1)}{n}. \quad (13)$$

Here n is the number of flare samples and E_{\min} is the minimum value of energy of the observed flares. Because of the incompleteness of the energy coverage of EDEN and K2 LC flares, we only calculate the power-law index α for K2 SC

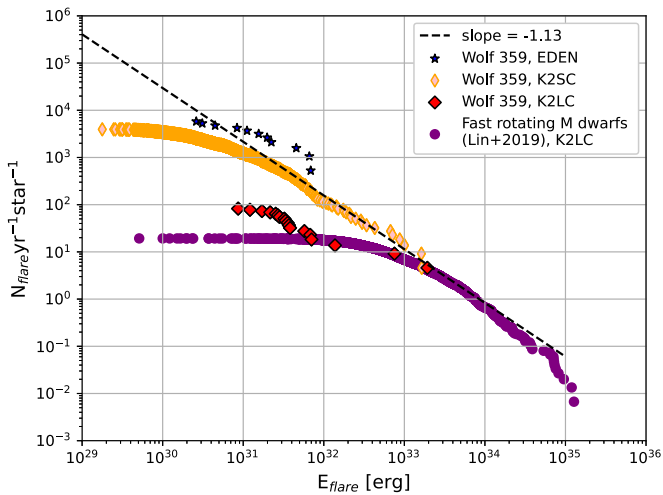


Figure 12. The flare frequency distribution of Wolf 359. The distributions of the EDEN flares (blue stars) and the K2 LC flares (red rhombuses) are incomplete due to a small amount of data. The K2 SC flares (orange rhombuses) give a relatively complete distribution that extends the frequency distribution of the rapidly rotating M dwarfs (purple circles) presented in the previous K2 LC flare study (Lin et al. 2019). The power-law index, $\alpha = 2.13 \pm 0.14$, has been estimated for the K2 SC flare frequency distribution using the maximum likelihood estimator derived by Clauset et al. (2009), and a slope $\beta = -1.13 \pm 0.14$ can therefore be obtained (black dashed line). Combining the fast rotating M dwarfs’ LC flares given by Lin et al. (2019) with Wolf 359 K2 SC flares, the estimated slope β aligns the flares from $E_f \approx 5 \times 10^{31}$ to 5×10^{33} erg.

flares. With $E_{\min} = 5.17 \times 10^{31}$ erg and $n = 70$, a value of $\alpha = 2.13 \pm 0.14$ can be obtained, and hence the slope $\beta = -1.13 \pm 0.14$ with $a = 38.61$. It is in good agreement with the power-law indices of $\alpha \approx 2.0$ – 2.4 estimated by Ilin et al. (2019) for the young late-type (from late-K to mid-M) flaring stars in young open clusters Pleiades (125 Myr) and Praesepe (630 Myr).

From Figure 12, one can see that the flare activity of Wolf 359 is at the same level of young, quickly rotating M dwarfs. The fitted power law also indicates that it will produce one flare with energy of the order of a few times 10^{31} erg each day. In comparison, the Sun would produce a flare of this magnitude about once every 2 months or so during solar maximum (Shibayama et al. 2013).

4.4. Potential Surface Habitability of the Wolf 359 System

High stellar activity may have a major, destructive impact on planetary atmospheres and volatile budget and has the potential to also directly impact surface life. Given the new insights into the stellar activity of Wolf 359, the fifth closest star to the Sun and a candidate exoplanet host, we will now briefly explore the potential impact of the observed stellar activity on putative habitable planets in this system. This discussion is, of course, only the first step—the detailed understanding of Wolf 359’s impact on potential habitable planets will likely benefit from space-based multiwavelength monitoring (e.g., Afanasev et al. 2019) and comprehensive modeling of possible types of atmospheres and the corresponding atmospheric loss rates.

Nevertheless, the data at hand already enable a cursory exploration of whether the flaring activity is expected to exclude surface habitability in the Wolf 359 system. Our observations confirm that Wolf 359 is a very active M dwarf

star. As shown by our observations, Wolf 359 displays extremely frequent (more than 1000 times per year) powerful flares (10^{31} – 10^{32} erg), similar in energy to the 1859 Carrington event in the solar system (e.g., Cliver & Dietrich 2013). Even worse, the detection superflares (with energies $\sim 10^{33}$ erg) in our K2 data and its occurrence rate in flare frequency distribution (see Figure 12) suggest that Wolf 359 likely drives, each year, several (~ 10 times) such superflares.

The flare activity of Wolf 359, even though extreme compared with the Sun, is typical for the active M dwarf planet host stars studied. For example, a recent TESS-based photometric study by Vida et al. (2019) of flare activity in Proxima Centauri—which is orbited by a habitable zone planet (Anglada-Escudé et al. 2016) with a likely mass of $1.7 M_{\oplus}$ (Bixel & Apai 2017)—found that Proxima also displays several superflares per year, similar to Wolf 359.

As there are yet insufficient data available to allow for detailed modeling of the flares’ impact on putative planets specifically around Wolf 359, we may turn to detailed modeling of a hypothetical Earth-like planet orbiting the flare star AD Leo (Segura et al. 2010). This study uses a one-dimensional atmospheric model to simulate the impact of the UV-A, UV-B, X-ray, and proton fluxes associated with a powerful (simulated) superflare event. Although the superflare has major impact on the atmospheric structure and composition, Segura et al. (2010) find that these changes are only short term and reversible. Therefore, they conclude that singular superflare events likely do not pose major threats to planetary habitability, although the cumulative impact of frequent lower-energy flares remains to be understood.

5. Conclusions

In this study, we present the K2 (LC and SC) and EDEN observations of Wolf 359 and identify 872 flares in total, 18 from K2 LC (17 have SC counterparts), 860 from K2 SC, and 11 from EDEN, using the flare detection method presented in Lin et al. (2019). These detected flares have energies in the range of $\sim 2 \times 10^{29}$ erg to 2×10^{33} erg. Wolf 359 is in the saturation phase of P_{rot} –FA relation and has a relatively strong flare activity when compared with other flaring M dwarfs. The spot-covering fraction—as derived from the rotational modulations—is at least $1.87\% \pm 0.59\%$ and may be significantly higher. Our data do not show evidence for the presence of a correlation between rotation phase and flare energy on Wolf 359, and several possibilities are discussed. A combination of the K2 and EDEN observations shows that the flare frequency distribution of Wolf 359 follows a power law of $dN/dE \propto E^{-\alpha}$, where $\alpha = 2.13 \pm 0.14$, and hence the cumulative frequency slope $\beta = -1.13 \pm 0.14$. According to this relation, the star will produce the flare with energy of the order of $\sim 10^{31}$ erg once each day, while the superflares with $E_f \geq 10^{33}$ erg could be generated ~ 10 times every year.

This analysis places Wolf 359 among the most magnetically active M dwarfs. It also shows the value and versatility of global ground-based observations like EDEN in the continuous monitoring of space weather effects of the host stars of exoplanets.

In summary, this study, in combination with the current data on the flare activity of Wolf 359 and other active planet host stars, suggests that the flare activity of Wolf 359 may not render its planetary system uninhabitable. Therefore, given its proximity and the fact that Wolf 359 is already a candidate exoplanet
















host, this system should remain an important target for habitable exoplanet searches.

We would like to thank the anonymous referee for the helpful comments for this work. This research was supported in part by grant No. 107-2119-M-008-012 of MOST, Taiwan, and grant No. 119/2017/A3 of FCDT of Macau, MSAR. The results reported herein benefited from collaborations and/or information exchange within NASA's Nexus for Exoplanet System Science (NExSS) research coordination network sponsored by NASA's Science Mission Directorate. B.V.R. thanks the Heising-Simons Foundation for support. Our study has used the data collected by the K2 mission. Funding for the K2 mission is provided by the NASA Science Mission directorate. This research made use of Lightkurve, a Python package for Kepler and TESS data analysis (Lightkurve Collaboration et al. 2018).

Facilities: SO:Kuiiper, VATT, Kepler/K2.

Software: Matplotlib (Hunter 2007), NumPy (Oliphant 2006), Pandas (McKinney 2010), Scipy (Virtanen et al. 2020).

ORCID iDs

Chia-Lung Lin  <https://orcid.org/0000-0001-5989-7594>
 Wen-Ping Chen  <https://orcid.org/0000-0003-0262-272X>
 Dániel Apai  <https://orcid.org/0000-0003-3714-5855>
 Alex Bixel  <https://orcid.org/0000-0003-2831-1890>
 Nestor Espinoza  <https://orcid.org/0000-0001-9513-1449>
 Aidan Gibbs  <https://orcid.org/0000-0002-9027-4456>
 Paul Gabor  <https://orcid.org/0000-0002-1315-9307>
 Thomas Henning  <https://orcid.org/0000-0002-1493-300X>
 Luigi Mancini  <https://orcid.org/0000-0002-9428-8732>
 Benjamin V. Rackham  <https://orcid.org/0000-0002-3627-1676>
 Martin Schlecker  <https://orcid.org/0000-0001-8355-2107>
 Jeremy Dietrich  <https://orcid.org/0000-0001-6320-7410>
 Quentin Jay Socia  <https://orcid.org/0000-0002-7434-0863>
 Asmita Bhandare  <https://orcid.org/0000-0002-1197-3946>
 Maximilian Häberle  <https://orcid.org/0000-0002-5844-4443>

References

Aarnio, A. N., Matt, S. P., & Stassun, K. G. 2012, *ApJ*, 760, 9
 Afanesev, D., Quintana, E., & Barclay, T. 2019, AAS Meeting, 233, 465
 Airapetian, V., Glöcer, A., Khazanov, V., et al. 2017, *ApJL*, 836, L3
 Anglada-Escudé, G., Amado, P. J., Barnes, J., et al. 2016, *Natur*, 536, 437
 Berdyugina, S. V. 2005, *LRSP*, 2, 8
 Bixel, A., & Apai, D. 2017, *ApJL*, 836, L31

Chang, H.-Y., Song, U. Y., Luo, A., et al. 2017, *ApJ*, 834, 92
 Chang, U.-Y., Lin, C.-L., Ip, W.-H., et al. 2018, *ApJ*, 867, 78
 Clauset, A., Shalizi, C. R., & Newman, M. E. J. 2009, *SIAMR*, 51, 661
 Cliver, E. W., & Dietrich, W. F. 2013, *JWSWC*, 3, A31
 Davenport, J. R. A., Covey, K. R., Clarke, R. W., et al. 2019, *ApJ*, 871, 241
 Doyle, J. G., & Butler, C. J. 1990, *A&A*, 235, 335
 Doyle, L., Ramsay, G., Doyle, J. G., et al. 2018, *MNRAS*, 480, 2153
 Doyle, L., Ramsay, G., Doyle, J. G., et al. 2019, *MNRAS*, 489, 437
 Engle, S. G., & Guinan, E. F. 2018, *RNAAS*, 2, 34
 Fuhrmeister, B., Liefke, C., & Schmitt, J. H. M. M. 2007, *A&A*, 468, 221
 Fuhrmeister, B., Liefke, C., Schmitt, J. H. M. M., & Reiners, A. 2008, *A&A*, 487, 293
 Fuhrmeister, B., Schmitt, J. H. M. M., & Hauschildt, P. H. 2005, *A&A*, 439, 1137
 Fuhrmeister, B., Schmitt, J. H. M. M., & Hauschildt, P. H. 2010, *A&A*, 511, A83
 Gershberg, R. E. 1972, *Ap&SS*, 19, 75
 Gibbs, A., Bixel, A., Rackham, B. V., et al. 2020, *AJ*, 159, 169
 Guinan, E. F., & Engle, S. G. 2018, *RNAAS*, 2, 2
 Hawley, S. L., Davenport, J. R., Kowalski, A. F., et al. 2014, *ApJ*, 797, 121
 Hawley, S. L., & Pettersen, B. R. 1992, *ApJ*, 378, 725
 Howard, W. S., Corbett, H., Law, N. M., et al. 2020, *ApJ*, 902, 115
 Howard, W. S., Tilley, M. A., Corbett, H., et al. 2018, *ApJL*, 860, L30
 Hunter, J. D. 2007, *CISE*, 9, 90
 Ilin, E., Schmidt, S. J., Davenport, J. R. A., et al. 2019, *A&A*, 622, A133
 Kirkpatrick, J. D., Henry, T. J., & McCarthy, D. W. 1991, *ApJS*, 77, 417
 Kowalski, A. F., Hawley, S. L., Holtzman, J. A., et al. 2010, *ApJL*, 714, L98
 Lefke, C., Fuhrmeister, B., & Schmitt, J. M. M. 2010, *A&A*, 514, A94
 Lightkurve Collaboration, Cardoso, J. V. M., Hedges, C., et al. 2018, Astrophysics Source Code Library, ascl:1812.013
 Lin, C.-L., Ip, W.-H., Hou, W.-C., et al. 2019, *ApJ*, 873, 97
 Maehara, H., Notsu, Y., Notsu, S., et al. 2017, *PASJ*, 69, 41
 Maehara, H., Shibayama, T., Notsu, Y., et al. 2012, *Natur*, 478, 485
 McKinney, W. 2010, in Proc. 9th Python in Sci.Conf., ed. S. vanderWalt & J. Millman, 51
 Oliphant, T. E. 2006, A Guide to NumPy (USA: Trelgol Publishing)
 Pavlenko, Ya. V., Jones, H. R. A., Lyubchik, Yu., Tennyson, J., & Pinfield, D. J. 2006, *A&A*, 447, 709
 Rackham, B. V., Apai, D., & Giampapa, M. S. 2018, *ApJ*, 853, 122
 Rietz, S., Stelzer, B., Damasso, M., et al. 2020, *A&A*, 637, A22
 Reid, I. N., Hawley, S. L., & Gizis, J. E. 1995, *AJ*, 110, 1838
 Reiners, A., & Basri, G. 2007, *ApJ*, 656, 1121
 Segura, A., Walkowicz, L. M., Meadows, V., Kasting, J., & Hawley, S. 2010, *AsBio*, 10, 751
 Shibata, K., & Magara, T. S. 2011, *LRR*, 8, 6
 Shibayama, T., Maehara, H., Notsu, S., et al. 2013, *ApJS*, 209, 5
 Smith, J. C., Stumpe, M. C., Van Cleve, J. E., et al. 2012, *PASP*, 124, 1000
 Stumpe, M. C., Smith, J. C., Van Cleve, J. E., et al. 2012, *PASP*, 124, 985
 Tuomi, M., Jones, H. R. A., Butler, R. P., et al. 2019, arXiv:1906.04644
 Vanderburg, A., & Johnson, J. A. 2014, *PASP*, 126, 948
 Vida, K., Kóvári, Z., Pál, A., et al. 2017, *ApJ*, 841, 124
 Vida, K., Oláh, K., Kóvári, Z., et al. 2019, *ApJ*, 884, 160
 Virtanen, P., Gommers, R., Oliphant, T. E., et al. 2020, *NatMe*, 17, 261
 Weinberger, A. J., Boss, A. P., Keiser, S. A., et al. 2016, *AJ*, 152, 24
 Wu, C.-J., Ip, W.-H., & Huang, L.-C. 2014, *ApJ*, 798, 92
 Yadav, R. K., Gastine, T., Christensen, U. R., et al. 2015, *A&A*, 573, A68
 Yang, H., Liu, J., Gao, Q., et al. 2017, *ApJ*, 849, 36